A Family of Electronically Reconfigurable Nanodevices — Source link ⌞↗⌟

Jianhua Yang, Julien Borghetti, David Murphy, Duncan Stewart ...+1 more authors

Institutions: Hewlett-Packard

Related papers:

- Memristive switching mechanism for metal/oxide/metal nanodevices.

- The missing memristor found

- Redox-Based Resistive Switching Memories – Nanoionic Mechanisms, Prospects, and Challenges

- Nanoionics-based resistive switching memories

- Atomic structure of conducting nanofilaments in TiO2 resistive switching memory

Summer June 2, 2009

A Family of Electronically Reconfigurable Nanodevices

Jianhua Yang, *University of Massachusetts - Amherst*
Julien Borghetti
David Murphy
Duncan Stewart
R Stanley Williams

A Family of Electronically Reconfigurable Nanodevices

By *J. Joshua Yang, Julien Borghetti, David Murphy, Duncan R. Stewart,* and *R. Stanley Williams*

Moore's law will come to an end in a decade or so and the emphasis in electronics design will have to shift to devices that are not just increasingly infinitesimal but increasingly capable. Here, we demonstrate the concept and realization of a class of such nanodevices with extremely simple structures, reconfigurable two-terminal electronic circuit elements that behave as networks of memristive switches[1–3] and rectifiers in parallel and series combinations, based on the physical properties of a metal/oxide/metal system. The two metal/semiconductor contacts can be either rectifying or conductive, depending on the concentration of dopants at the respective interface,[4] which provides four different current–voltage characteristics. By forcing charged dopants into or out of the interface region with an applied electric field pulse, devices can be switched from one type of stable operation to another in five different ways. A family of devices built to express these properties displays a rich set of behaviors that provide new opportunities for nanoelectronics.

Over 30 years ago Leon Chua proposed the existence of a new class of passive circuit elements, memristors and memristive devices, to complement the resistor, capacitor, and inductor.[1,2] However, it was not until this year that a simple device physics model[3] and experimental device examples[4] demonstrated that memristance arises naturally in nanoscale semiconductor films in which solid-state electronic and ionic (dopant) transport are coupled under an external electrical bias. Although there had been many prior reports of anomalous hysteretic behavior in the current–voltage (*I–V*) characteristics of metal/dielectric/metal systems, the connection to memristive dynamics was not made. In part, this was caused by the fact that most of the previous devices that had been built and tested also possessed some very strong nonlinear electronic transport property,[5–13] such as tunneling or rectification, that masked the memristive behavior of these systems. Here, we demonstrate that intentionally combining these two properties that are now associated with metal-semiconductor interfaces, namely memristive switching and nonlinear Schottky-like rectification, enables us to build a family of reconfigurable electronic devices[14] with interesting and useful properties for switching, memory, and logic.

We have reported reversible bi-polar resistive switching in Pt/TiO$_2$/Pt two-terminal nanodevices, which we modeled as a memristor in parallel with a rectifier.[4] The switching mechanism involved changes to the Schottky-like barrier at a Pt/TiO$_2$ interface caused by the drift of positively charged oxygen vacancies (V$_O$s) under an applied electric field. These nanoscale switches may enable a new type of nonvolatile random access memory (RAM)[15–20] and analog switching for neuromorphic computing.[21] Here, we show that the previously reported nanoswitches are actually just one member in a family of memristively switched reconfigurable devices that behave as a network of parallel and series memristors and rectifiers. The entire family of compound circuit elements can be constructed from a relatively simple metal/oxide/metal framework that yields different two-terminal devices depending on the initial distribution of oxygen vacancies. These unique devices will enhance the toolkit of circuit designers and may allow new nanoelectronic architectures in a variety of applications including memory,[22,23] logic,[24,25] synaptic computing,[26] and other circuits.[27–29]

The general concept for the reconfigurable circuit elements is illustrated in Figure 1. A device consists of a titanium oxide layer sandwiched by two metal (in this case Pt) electrodes. Each device has two metal/oxide interfaces that influence the electronic transport perpendicular to the tri-layer. The oxygen vacancies in TiO$_2$ are n-type dopants,[30] transforming the wide bandgap oxide into an electrically conductive doped semiconductor. Metal-semiconductor contacts are typically Ohmic in the case of very heavy doping, and blocking or rectifying (Schottky-like) in the case of low doping,[31] so the concentration of V$_O$s at an interface determines its electrical transport behavior. In Figure 1, we classify four different quasi-static electrical characteristics or end-states of the devices, i.e., *forward rectifier, reverse rectifier, shunted rectifier* (characterized by a lower resistance, symmetric *I–V* plot) and *head-to-head rectifiers* (a high resistance or effectively open state). Which quasi-static state dominates is determined by the distribution of V$_O$s in the thin film of TiO$_2$ between the two Pt electrodes, and by the choice of the circuit ground. These states will be stable as long as the voltage biases applied to the devices are small enough or fast enough that the distribution of the V$_O$s is not perturbed.

However, the vacancies are mobile under a high enough electric field ($\sim 10^6$ V cm^{-1}),[32] which is readily achieved with only a few volt bias when the film has a nanoscale thickness. The reconfiguration of the semiconductor doping profiles due to the drift of V$_O$s under the electric field can in principle lead to six different electrical switching transitions between pairs of the four device states classified above, as illustrated in Figure 1. *Shunting* is exemplified by the switching between the forward rectifier and the shunted rectifier. The bottom interface of the junction is heavily doped and remains Ohmic (or at least highly conductive) with negligible changes during the switching. The transition is initiated when a sufficiently large negative bias applied on the top electrode (TE) attracts positively charged V$_O$s to the top interface, switching the device from a forward rectifier to a shunted rectifier.
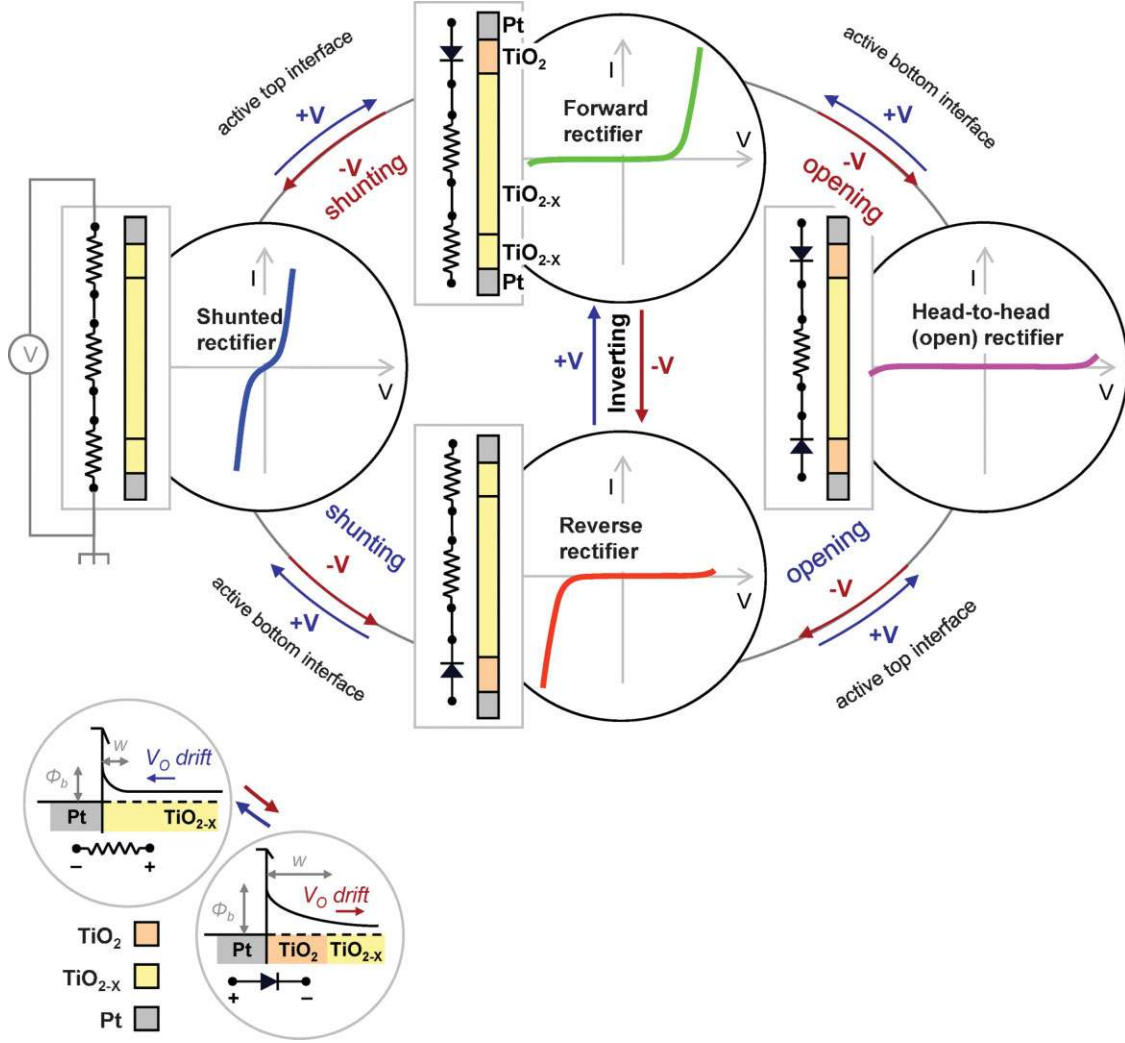
Figure 1. A family of device states exists when two dynamic metal (Pt)/semiconductor (TiO_x) junctions are operated in series. Schematic drawings of the four current–transport end-states and the modes of switching between them: the *I–V* characteristics and the corresponding oxygen vacancy (V_O) profiles in the oxide layers are shown for the quasi-static states, with orange indicating lower V_O concentrations (semi-insulating TiO_2). A high concentration of vacancies at the metal-semiconductor interface (yellow = TiO_{2-x}) produces an essentially Ohmic contact, whereas a low concentration yields a Schottky-like rectifier or blocking contact (lower left). Positively charged V_Os drift toward or away from an interface depending on the as-fabricated V_O distribution and the applied voltage polarity, resulting in switching between different states.

An opposite bias repels the V_Os to switch the device back to the forward rectifier. Of course, the transitions between a reverse and a shunted rectifier can also be called shunting, as labeled in Figure 1. *Opening* is switching between a forward or reverse rectifier and a head-to-head rectifier. In the reverse rectifier case, the bottom interface remains unchanged and only the top interface is actively switched. Conversely, the forward rectifier case has an active bottom interface. In both cases, the unchanged interface (with very few V_O dopants) remains rectifying during switching. *Inverting* is different; it involves simultaneous and opposite changes at both interfaces, resulting in switching between a reverse rectifier and a forward rectifier. The last switching type, between the shunted rectifier and the head-to-head rectifier, has not been observed to date in a real device. The reason for this is clear, since it would require the V_Os to drift in opposite directions simultaneously at the two interfaces.

The two interfaces of the device are the keys to both the transport and switching. We first performed experiments (Fig. 2) to demonstrate the role of V_Os in modulating the properties of the interfaces. Figure 2a presents an optical microscope image of several devices that consist of Pt TEs and bottom electrodes (BEs) separated vertically by a blanket titanium oxide layer. The titanium oxide layer is actually a bi-layer consisting of a very thin (4 nm) nearly stoichiometric TiO_2 layer and a thicker (120 nm) TiO_{2-x} layer with a high concentration of V_Os (Fig. 2b). The TiO_{2-x} layer is an n-type semiconductor with a carrier concentration of $\sim 10^{19} \, cm^{-3}$ as determined from Hall measurements (see Supporting Information Fig. S1, S2). Any pair of electrodes in Figure 2a form a two-terminal device as schematically shown in Figure 2b, from which an *I–V* curve can be obtained (Fig. 2c). The *I–V* curve between two BEs (e.g., BE1 and BE3) is linear (red), revealing Ohmic contacts at both the
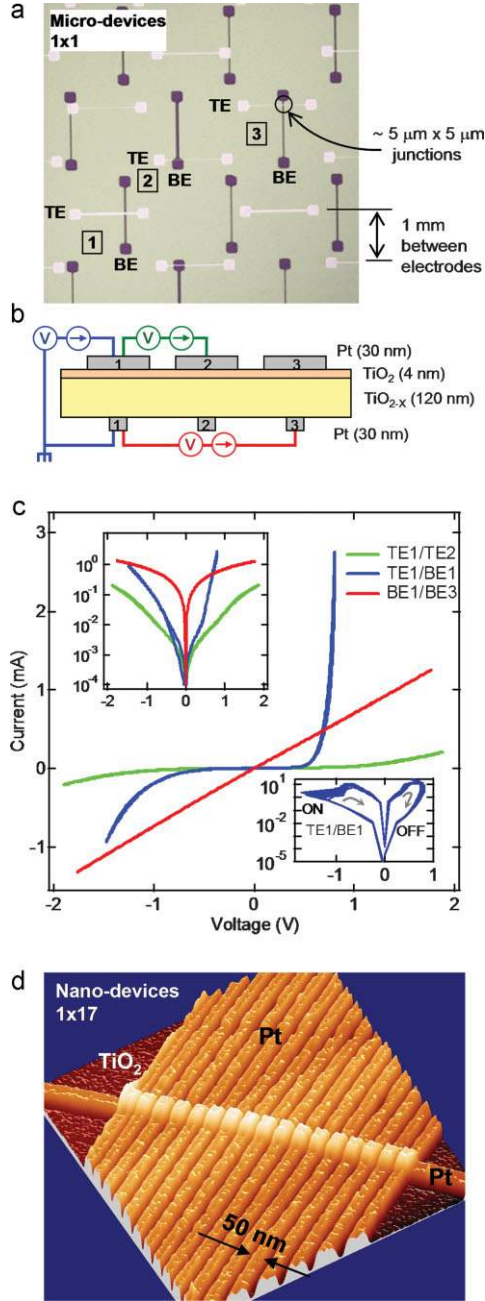
Figure 2. Nonlinear electronic transport is controlled by the oxygen vacancy (V_O) doped metal/oxide interfaces. a) Optical microscope image of a micro-device sample. The dumbell-shaped BEs (BE, vertical) and TEs (TE, horizontal) are separated by the blanket Ti oxide layer (light blue). b) Schematic drawing. The oxide is a 4 nm TiO_2/120 nm TiO_{2-x} sputter-deposited bilayer. Current–voltage I–V measurements were made between pairs of the electrodes. c) Linear and semi-log I–V plots. Red: Ohmic conduction between two bottom Pt/TiO_{2-x} electrodes. Green: highly resistive and symmetric conduction between two top Pt/TiO_2 electrodes. Blue: forward rectification from a top Pt/TiO_2 electrode to the bottom Pt/TiO_{2-x} electrode. The lower right inset shows reversible switching operation with a zero bias resistance ratio of ∼1000 for a device defined by electrodes TE1 and BE1. d) AFM images of 1×17 crosspoint nanodevices as used for the shunting and inverting transition measurements. The top and BEs for all devices are Pt and the insulating layer is a blanket film of TiO_2 with an engineered distribution of oxygen vacancies.

Pt/TiO_{2-x} interfaces. In contrast, the I–V curve between two TEs (e.g., TE1 and TE2) is symmetric and nonlinear (green), revealing blocking contacts at both Pt/TiO_2 interfaces. The much lower current between the TEs compared to the BEs shows that the blocking interfaces dominate the electrical transport. A rectifying I–V (blue curve) is obtained between electrodes TE1 and BE1, consistent with the fact that the corresponding device has one blocking (Pt/TiO_2) interface and one Ohmic (Pt/TiO_{2-x}) interface. Reversible switching I–V loops between TE1 and BE1 similar to those previously reported are shown as the lower inset to Figure 2c.

Crosspoint devices have been built to demonstrate the device concepts shown in Figure 1. Figure 2d presents an atomic force microscope (AFM) image of a 1×17 set of nanodevices (50 nm × 50 nm) as used for the shunting and inverting transition measurements. An ultra-high density two-dimensional array of such configurable memristive nanodevices suitable for memory or logic applications has also been built, as shown in the Supporting Information (Fig. S3).

The as-fabricated state of a junction, i.e., the initial V_O profile, in large degree determines the switching character of the device. The initial V_O profile can be controlled by engineering the structure and/or the fabrication conditions of the device (see Supporting Information). In the following, we demonstrate three types of switching in real devices.

Figure 3a presents the experimental data for a *shunting* transition. The BE is grounded and the voltage is applied to the TE for all electrical measurements in this study. The device was fabricated to have a very asymmetric distribution of V_Os, with the top interface having a much smaller concentration than the bottom interface which thus remains Ohmic during switching. The active region is the top interface, governing the electronic transport of the junction and the switching. A positive bias on the TE repels the positively charged V_Os from the top interface and switches the device from a conducting to a rectifying state (green I–V curves). A negative bias on the TE attracts the V_Os to the top interface and shunts the rectifier at the top interface, switching the device to a symmetric higher conductance state (blue). Depending on the length and magnitude of the bias, the device can be configured continuously between the two end states. This is exemplified in Figure 3a, where the final two symmetric I–V states have a higher resistance than the first two. We have previously demonstrated that a simple equivalent network (Fig. 3a) with a memristor in parallel with a rectifier describes the switching and end-state I–V behavior of such a device reasonably well.[4]

The electrical data for the *opening* transition is shown in Figure 3b. The two interfaces of this device are also engineered to be asymmetric. The more resistive top interface remains rectifying during the transition and the active region is the bottom interface. A negative voltage sweep to −8V pulls positive V_Os away from the bottom interface and leaves the device in a very high resistance head-to-head or open state, as revealed by the quasi-static I–V curves (pink). The positive bias transition sweep to +5 V (blue) then switches the bottom interface to an Ohmic state, and the electrical transport of the device is again limited by the rectifying top interface (green end-state curve). Expanded-scale I–V curves for both head-to-head and forward-rectifier states are shown as an inset to Figure 3b. The equivalent circuit for this device adds an anti-parallel rectifier in series with the shunting
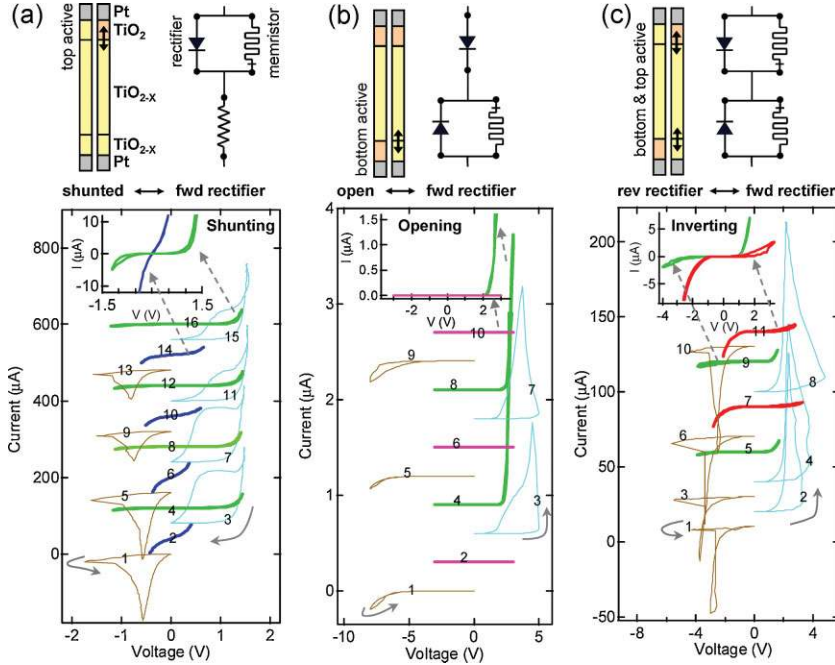
Figure 3. Experimental current–voltage data for shunting a), opening b), and inverting c) transitions, the end states after switching the devices, and their corresponding equivalent circuits. For each transition type, the I–V curves are numbered in the sequence in which they were collected. These I–V curves are shown with a certain current offset for clarity. Brown and cyan I–V curves represent negative and positive transition voltage sweeps (on TE), respectively. After each transition sweep (negative or positive), an interrogation I–V was collected to determine the device state after switching. The upper-left insets display the two end states corresponding to each transition type. a) Shunting transition data from a 50 nm × 50 nm nanodevice. The device is switched to a forward rectifier with a positive bias, as verified by the green I–V characteristic. The device is switched to a symmetric low resistance state with a negative bias (verified by the blue I–V). Depending on the magnitude of the bias, the device can be switched continuously between the end states, with higher resistances shown by the smaller loops for the last two shunting-transition sweeps. The equivalent network for this device consists of a rectifier in parallel with a memristor. b) Opening transition data from a 5 μm × 5 μm device, to yield a current high enough for low noise measurements. The device is switched to the head-to-head or open state with a negative bias (interrogation curves in pink). The device is switched to the forward rectifier state with a positive transition bias (end-state shown by green I–V curves). The equivalent network for this device consists of an intrinsic rectifier in series with a shunting-transition device. c) Inverting transition data from a 50 nm × 50 nm device. The rectifying direction of the test I–V curve (green or red) is inverted after each transition induced by a positive (cyan) or negative bias (brown). The equivalent circuit consists of two head-to-head shunting-transition devices in series.

transition device of Figure 3a. An opening-transition device is ideal as a bit cell in a crossbar memory, since it effectively eliminates the problem of cross-talk or current sneak-paths in this highly interconnected architecture.[33] In addition, the operating power for this type of device is extremely low. We anticipate good scalability of this structure, with switching and reading at the nA current level for nanoscale devices based on the μA currents used to switch the microscale device in Figure 3b (used for this demonstration to prove low noise operation).

Figure 3c presents the electrical data for the *inverting* transition. This device was carefully fabricated with an almost symmetric V_O concentration profile. With a positive voltage sweep on the TE, V_Os are repelled from the top interface and simultaneously attracted to the bottom interface, resulting in a higher concentration of V_Os at the bottom and a forward-rectifier state (green I–V curves). A negative transition sweep reverses the V_O profile in the oxide layer

and switches the device to the reverse-rectifier state (red I–V curves). The equivalent network (inset in Fig. 3c) for an inverting-transition device is just two head-to-head shunting-transition devices in series.

In addition to the above transitions between pairs of the four end-states, transitions involving three end-states are also possible and lead to interesting triply-configurable devices that may find unique applications in some new electronic circuits, e.g., synaptic computing. Figure 4 exemplifies such a device that has the same equivalent network as that of the *inverting*-transition device, except in this case there are two types of transitions: shunting to switch the device reversibly from either a forward or reverse rectifier to the shunted state, and inverting to switch the device from the forward to the reverse rectifier state and back.

We have introduced a family of reconfigurable nanodevices based on the interaction between the memristive switching and recti-fication properties at the two interfaces of metal/oxide/metal crosspoint devices. Four different I–V end states are possible depending on the transport properties at the two interfaces of a crosspoint, and it is possible at present to build three types of devices that exhibit transitions between pairs of these states by controlling the initial distribution of V_Os in the oxide layer. An interesting triply-configurable device has also been demonstrated. These devices may find promising applications for their ability to be field configured into a particular state (forward or reverse rectifier, conductor or open) or for their actual switching properties as the transition between states under an applied voltage bias.

Experimental

Metallic Pt and Ti layers were deposited by electron-beam evaporation at room temperature. The TiO$_2$ film in every device is a blanket layer covering the entire wafer, and the junction is defined by the material at the crosspoint between the bottom and the TEs. The TiO$_2$ films were fabricated by sputter-deposition from a TiO$_2$ target. The TiO$_2$ layers for the devices shown in Figure 4 were 30–50 nm thick. The 120 nm TiO$_{2-x}$ layer in Figure 2 and the 90 nm TiO$_{2-x}$ layer in Figure S1 of Supporting Information were deposited by reactive sputtering from a Ti target with Ar and 5% O$_2$ gas mixture. The substrate temperature was held at 250 °C during deposition of the Ti oxide layer. The Ti (2 nm adhesion layer) + Pt (9 nm) electrode used for the 50 nm × 50 nm nanojunctions was patterned by ultraviolet-nanoimprint lithography. Details of the nanoimprint fabrication can be found in the reference: *Nano Lett.* 2004, 4, 1225. The Ti (5 nm adhesion layer) + Pt (15–30 nm) electrode used for the micro-junctions (5 μm × 5 μm) was fabricated using a metal shadow mask. The V_O profile can be controlled by engineering the structure and/or the fabrication conditions of the device, such as the deposition gas species and pressure, the presence of an annealing step and its environment and depositing a reactive metal (e.g., Ti) at one or both electrode/TiO$_2$
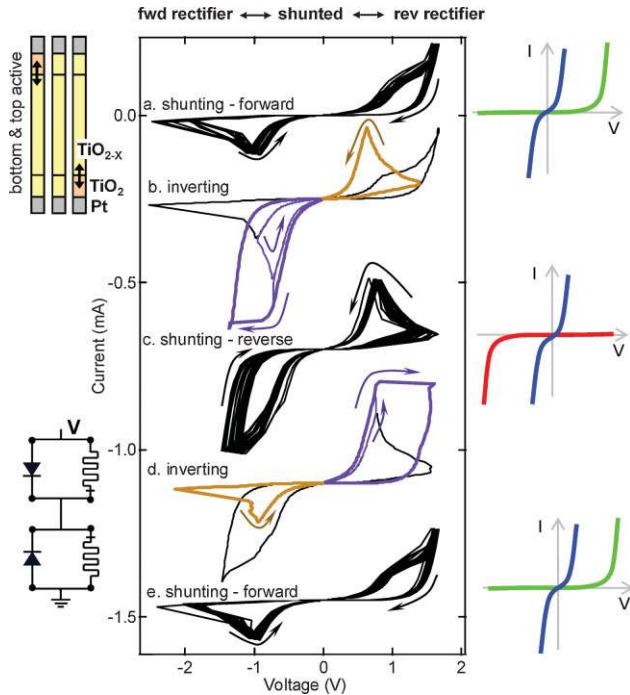
Figure 4. Triply configurable device involving three end-states (forward, shunted, and reverse rectifier) instead of just two end-states. The junction area is 50 nm × 50 nm. The transition sweeps are lettered in sequence: a) 20 shunting transition cycles from the forward rectifier state; b) application of larger negative transition sweeps (purple) cause the device to invert from the forward to a reverse rectifier state; c) 20 shunting transition cycles from the reverse rectifier state; d) application of larger positive transition sweeps (purple) cause the device to invert from the reverse to the forward rectifier state; and e) 20 more shunting transition cycles from the forward rectifier state. The resistance ratio for either rectifier state to the shunted state at +0.5 V is about 1000.

interfaces to create a high density of V_Os. A single irreversible forming step was necessary for the as-prepared (virgin) devices before they exhibited repeatable switching cycles; the forming usually occurred at approximately +/−8 V and 10 µA. The switching polarity of the device is determined by the initial oxygen vacancy profile rather than the forming step. See ref. [34] for details. An HP 4156 semiconductor parameter analyzer was used for the electrical characterization with the 4-probe DC measurement method. The BEs of the junctions were grounded during all the electrical measurements.

[1] L. O. Chua, *IEEE Trans. Circuit Theory* **1971**, *CT-18*, 507.
[2] L. O. Chua, S. M. Kang, *Proc. IEEE* **1976**, *64*, 209.
[3] D. B. Strukov, G. S. Snider, D. R. Stewart, R. S. Williams, *Nature* **2008**, *453*, 80.
[4] J. J. Yang, M. D. Pickett, X. Li, D. A. A. Ohlberg, D. R. Stewart, R. S. Williams, *Nat. Nanotechnol.* **2008**, *3*, 429.
[5] M. N. Kozicki, M. Park, M. Mitkova, *IEEE Trans. Nanotechnol.* **2005**, *4*, 331.
[6] A. Beck, J. G. Bednorz, C. Gerber, C. Rossel, D. Widmer, *Appl. Phys. Lett.* **2000**, *77*, 139.
[7] M. J. Rozenberg, I. H. Inoue, M. J. Sanchez, *Appl. Phys. Lett.* **2006**, *88*, 033510.
[8] S. Q. Liu, N. J. Wu, A. Ignatiev, *Appl. Phys. Lett.* **2000**, *76*, 2749.
[9] M. Janousch, G. I. Meijer, U. Staub, B. Delley, S. F. Karg, B. P. Andreasson, *Adv. Mater.* **2007**, *19*, 2232.
[10] J. R. Jameson, Y. Fukuzumi, Z. Wang, P. Griffin, K. Tsunoda, G. I. Meijer, Y. Nishi, *Appl. Phys. Lett.* **2007**, *91*, 112101.
[11] A. Baikalov, Y. Q. Wang, B. Shen, B. Lorenz, S. Tsui, Y. Y. Sun, Y. Y. Xue, C. W. Chu, *Appl. Phys. Lett.* **2003**, *83*, 957.
[12] R. L. McCreery, *Chem. Mater.* **2004**, *16*, 4477.
[13] S. Seo, M. J. Lee, D. H. Seo, E. J. Jeoung, D.-S. Suh, Y. S. Joung, I. K. Yoo, I. R. Hwang, S. H. Kim, I. S. Byun, J.-S. Kim, J. S. Choi, B. H. Park, *Appl. Phys. Lett.* **2004**, *85*, 5655.
[14] J. J. Yang, J. Borghetti, D. Murphy, D. R. Stewart, R. S. Williams, "Reconfigurable Nanodevice Family Combining Memristive Switching and Rectification", presented at the *9th Annual Nonvolatile Memory Technology Symposium*, Pacific Grove, CA, November 11–14, **2008**.
[15] G. I. Meijer, *Science* **2008**, *319*, 1625.
[16] K. Terabe, T. Hasegawa, T. Nakayama, M. Aono, *Nature* **2005**, *433*, 47.
[17] R. Waser, M. Aono, *Nat. Mater.* **2007**, *6*, 833.
[18] K. Szot, W. Speier, G. Bihlmayer, R. Waser, *Nat. Mater.* **2006**, *5*, 312.
[19] Y. Watanabe, J. G. Bednorz, A. Bietsch, C. Gerber, D. Widmer, A. Beck, S. J. Wind, *Appl. Phys. Lett.* **2001**, *78*, 3738.
[20] R. Muenstermann, R. Dittmann, K. Szot, S. Mi, C. Jia, P. Meuffels, R. Waser, *Appl. Phys. Lett.* **2008**, *93*, 023110.
[21] C. Mead, *Analog VLSI and Neural Systems*, Addison-Wesley, Reading, MA **1989**.
[22] J. E. Green, J. W. Choi, A. Boukai, Y. Bunimovich, E. Johnston-Halperin, E. DeIonno, Y. Luo, B. A. Sheriff, K. Xu, Y. S. Shin, H.-R. Tseng, J. F. Stoddart, J. R. Heath, *Nature* **2007**, *445*, 414.
[23] S. H. Jo, K.-H. Kim, W. Lu, *Nano Lett.* **2009**, *9*, 870.
[24] C. P. Collier, E. W. Wong, M. Belohradský, F. M. Raymo, J. F. Stoddart, P. J. Kuekes, R. S. Williams, J. R. Heath, *Science* **1999**, *285*, 391.
[25] J. Borghetti, Z. Li, J. Straznicky, X. Li, D. A. A. Ohlberg, W. Wu, D. R. Stewart, R. S. Williams, *PNAS* **2009**, *106*, 1699.
[26] G. S. Snider, *Nanotechnology* **2007**, *18*, 365202.
[27] Z. Zhong, D. Wang, Y. Cui, M. W. Bockrath, C. M. Lieber, *Science* **2003**, *302*, 1377.
[28] W. Lu, C. Lieber, *Nat. Mater.* **2007**, *6*, 841.
[29] J. R. Heath, P. J. Kuekes, G. S. Snider, R. S. Williams, *Science* **1998**, *280*, 1716.
[30] P. Knauth, H. L. Tuller, *J. Appl. Phys.* **1999**, *85*, 897.
[31] E. H. Rhoderick, R. H. Williams, *Metal–Semiconductor Contacts*, 2nd Ed, Oxford Science Publications, Oxford **1988**.
[32] J. Blanc, D. L. Staebler, *Phys. Rev. B* **1971**, *4*, 3548.
[33] J. C. Scott, *Science* **2004**, *304*, 62.
[34] J. J. Yang, F. Miao, M. D. Pickett, D. A.A. Ohlberg, D. R. Stewart, C. N. Lau, R. S. Williams, *Nanotechnol.* **2009**, *20*, 215201.